Journal of Power Sources 268 (2014) 824–830

Contents lists available at ScienceDirect

Journal of Power Sources

journal homepage: www.elsevier.com/locate/jpowsour

Preparation and characterization of carbon-supported PtOs electrocatalysts via polyol reduction method for methanol oxidation reaction

Zuopeng Li [a], Muwu Li [b], Mingjia Han [b], Jianhuang Zeng [b, *], Yuexia Li [c], Yanqin Guo [b], Shijun Liao [b]

[a] Institute of Applied Chemistry, Shanxi Datong University, No. 5 Xingyun Street, Datong 037009, China
[b] School of Chemistry and Chemical Engineering, South China University of Technology, Guangdong Key Lab for Fuel Cell Technology, Guangzhou 510641, China
[c] North University of China, Shuozhou, No. 65 Changning Street, Shuozhou 036000, China

HIGHLIGHTS

- A polyol reduction approach was employed to prepare highly active PtOs/C for methanol oxidation.
- The catalysts' physical characteristics correlated with their electrochemical performances.
- Activity improvement was attributed to a mix of nanoparticles, high metallic Os and small sizes.
- The mass and specific activity of PtOs-2/C is 528 mA mg^{-1}_{PtOs} and 0.98 mA cm^{-2}, respectively.

ARTICLE INFO

Article history:
Received 15 April 2014
Received in revised form
8 June 2014
Accepted 23 June 2014
Available online 7 July 2014

Keywords:
PtOs electrocatalysts
Methanol oxidation reaction
Polyol
Co-deposition
Sequential deposition

ABSTRACT

A polyol reduction approach was employed to prepare carbon-supported PtOs/C electrocatalysts (PtOs-1/C was obtained via the co-reduction of H_2PtCl_6 and K_2OsCl_6 precursors and PtOs-2/C was obtained via a sequential deposition method in which Pt was deposited on the preformed Os nanoparticles). The home-made electrocatalysts were extensively characterized via transmission electron microscopy, thermogravimetric analysis, X-ray diffraction, and X-ray photoelectron spectroscopy. The evaluation results of the catalytic activities obtained via cyclic voltammetry, CO stripping voltammetry, and chronoamperometry showed that the successively reduced PtOs-2/C out-performed PtOs-1/C in terms of specific/mass activity (528 mA mg^{-1}_{PtOs} and 0.98 mA cm^{-2}) and CO tolerance in room temperature methanol electrooxidation reaction. The physical characteristics of the electrocatalysts correlated well with their electrochemical performances. The higher activity of PtOs-2/C was attributed to a combination of factors, such as a mix of nanoparticles (isolated Os, PtOs alloys or bimetallic nanoparticles), higher metallic Os content, and smaller particle sizes.

1. Introduction

Among various types of low-temperature fuel cells, direct methanol fuel cell (DMFC) is the most promising as a power source for portable products that require low power density but high energy density (e.g., 4G phones, iPad, and notebook PCs) [1–3]. Their ability to operate at relatively low temperatures and quick start-up characteristics (considering methanol is used directly without the need for fuel reforming) is comparable with those of H_2/O_2 polymer electrolyte membrane fuel cells based on hydrogen oxidation [4–7]. To date, the failure in developing highly efficient electrocatalysts for methanol oxidation has slowed down the development of DMFCs. This obstacle is caused by the slow oxidation kinetics of methanol oxidation at the Pt anode, which involves a complex network of reactions with many possible side products (6-electrons are transferred whereas only 2-electrons are transferred in hydrogen oxidation) especially at low operating temperatures [8]. More active catalysts or a larger quantity of catalyst are required in the case of DMFCs [9,10]. The situation is made worse by the rapid deactivation of the active catalyst surface by CO-like reaction

* Corresponding author. Tel.: +86 20 39099665.
E-mail address: cejhzeng@scut.edu.cn (J. Zeng).

http://dx.doi.org/10.1016/j.jpowsour.2014.06.122
0378-7753/

intermediates that are formed during the stepwise dehydrogenation of methanol [11]. Pt is therefore often alloyed with an oxophilic metal to increase its CO tolerance. Among bimetallic Pt catalysts, the Pt–Ru system is best known for its activity in the electrochemical methanol oxidation reaction (MOR) [12–15]. However, the efficiency of DMFCs operating on Pt–Ru is still insufficient for most practical purposes. Furthermore, the supply of Ru and the toxicological effect of Ru remain an issue [16]. Therefore, alternative Ru-free DMFC anode catalysts are still being explored [17].

Earlier transition metals are the most oxophilic elements based on their gas-phase dissociation energies. Moreover, Os is more oxophilic than Ru and is known to adsorb water in acidic solutions at potentials that are slightly more negative than Ru [18]. Os and Os-based catalysts (other than Pt) are catalytically inactive for methanol oxidation, as reported by Atwan [19]. Several studies were done on PtOs electrocatalysts for methanol oxidation, CO oxidation, and formic acid oxidation [20–24]. Liu and Huang prepared Pt–Os (3:1)/C catalysts (2.2 nm) via the thermal decomposition of metallic carbonyl cluster, and this catalyst showed a superior electrocatalytic activity to formic acid oxidation compared with Pt/C catalyst because of the fine dispersion of Pt–Os and the bifunctional effect [20]. Carbon-supported Pt–Os electrocatalysts prepared via different methods were compared with Pt/C, and PtOs (9:1)/C heat-treated under H_2 at 500 °C showed the best performance for CO oxidation because of the reduction of inactive Pt and Os surface oxide phases [21]. In a study on PtM_yO_x (M = Sn, Mo, Os, or W) electrodes, the Os-added electrode showed dissatisfactory methanol oxidation performance because volatile OsO_4 was formed during the calcination process [22]. Electrochemically co-deposited Pt–Os electrodes have shown enhanced catalytic activity over Pt at potentials beyond 0.2 V versus Ag/AgCl (3 M NaCl) because of more oxophilic behaviors of Os [24]. However, the formation of OsO_2 in high potentials could lead to the loss of active OH species. A carbon-supported Pt–Os bimetallic catalyst (2.2 nm) with a Pt/Os atomic ratio of 3:1 prepared via the carbonyl complexes route has been reported to exhibit enhanced activity for MOR than commercially available Pt/C and Pt–Ru (1:1)/C, and the enhancement has been ascribed to the combination of bifunctional mechanism and the electronic effect [23]. Moore et al. prepared Os/C and Pt–Os/C by thermally treating three types of Os complexes at solely reductive conditions [25]. Although Os/C and Pt–Os/C (5 nm–6 nm) gave open circuit potentials indicative of thermodynamically favorable methanol oxidation, the kinetics of these oxidations are too low to be of practical importance. Therefore, although Os is oxophilic in nature, the reported results on PtOs electrocatalysts for methanol oxidation were by no means consistent. The preparation method has a strong influence on the resulting catalyst performance. The polyol approach, which is often used in fuel cell preparation, has been used to successfully synthesize sub 5 nm nanoparticles with a narrow size distribution [26]. However, to the best of our knowledge, the polyol method has not been applied for the preparation of PtOs electrocatalysts. Studies that focus on the in-depth analysis between comparable preparation methods and the resulting catalysts performances are limited. Thus, in this work, PtOs colloids were synthesized via different deposition sequences (co-deposition versus sequential deposition) and were then harvested using carbon as supported electrocatalysts for methanol oxidation reaction. The Pt/Os atomic ratio was preset at 3:1 because this ratio has been regarded as the optimal one based on published results in literature [20,23]. The catalysts prepared via the polyol method were ~2 nm–2.5 nm in size and behaved quite differently toward MOR. The catalysts prepared in this work need no further post-heat-treatment and the preparative method itself is relatively straightforward (without usage of organic complexes). However, the addition of Os as PtOs bifunctional catalysts has inherent disadvantages since OsO_4 is a toxic gaseous species.

2. Experimental

2.1. Chemicals and materials

Potassium hexachloroosmate (K_2OsCl_6), chloroplatinic acid (H_2PtCl_6) from Aldrich, ethylene glycol, sodium hydroxide, sulfuric acid (95%–97%), ethanol, and methanol from Merck were used as received without further purification. K_2OsCl_6 and H_2PtCl_6 were prepared with 0.05 M aqueous solutions for further use. The carbon support was Vulcan XC-72 (measured BET surface area of 228 $m^2\ g^{-1}$ and average particle size of 40 nm–50 nm) from Cabot. Filtered deionized water was used throughout the study.

2.2. Preparation of PtOs-1/C catalyst

PtOs-1 was prepared by co-depositing the corresponding precursors via a polyol method: 1 mL of 0.05 M K_2OsCl_6 and 3 mL of 0.05 M H_2PtCl_6 were added to a 100 mL round-bottom flask containing 50 mL of ethylene glycol, and the pH of the mixture was adjusted to around 9 by using 0.5 M NaOH solution. The mixture was heated at 120 °C in an oil bath under reflux with stirring for 8 h. A calculated amount of XC-72 carbon (254 mg) was added to the reaction mixture after cooling, and stirring was continued overnight. The Pt loading was predetermined to be 10 wt.% assuming a complete reduction of the Pt precursor. The total metal loading (PtOs), assuming a complete reduction of the Pt and Os precursors, is 13.4 wt.%. The suspension was then filtered to recover the solid, which was copiously washed with ethanol before drying in vacuum at 80 °C overnight.

2.3. Preparation of PtOs-2/C catalyst

PtOs-2 was prepared via a sequential deposition process, in which Os colloids were first synthesized via a hydrothermal method followed by the subsequent polyol deposition of Pt nanoparticles: 1 mL of 0.05 M K_2OsCl_6 was mixed with 25 mL of ethylene glycol, and the pH of the mixture was adjusted to around 9 by using 0.5 M NaOH solution. The mixture was then transferred to a Teflon-lined stainless steel autoclave (custom-made cylinder with 4 cm cross-sectional diameter and 50 mL internal volume) and placed inside an electric oven at 120 °C for 4 h. After the synthesis, the colloidal sols were transferred to a 100 mL round-bottom flask. To this flask containing colloidal Os sols, 3 mL of 0.05 M H_2PtCl_6 and 25 mL of ethylene glycol were added, and the pH of the mixture was again adjusted to around 9 by using 0.5 M NaOH solution. The rest of the preparation procedures followed the same as those in the preparation of PtOs-1/C.

2.4. Materials characterizations

The X-ray powder diffraction (XRD) patterns of the catalysts were recorded using a Rigaku D/Max-3B diffractometer (Shimadzu) with CuK_α radiation (λ = 1.5406 Å). The 2θ angles were scanned from 20° to 85° at 2° min^{-1}. The diffraction data was curve-fitted using a least square program provided by the equipment manufacturer. Thermogravimetric analysis (TGA) was conducted using a Thermal Analysis Instruments 2050 Analyzer in 100 mL min^{-1} continuous airflow to determine the metal loadings in the catalysts. Given that OsO_4 is a volatile and toxic gas [22,25], the analysis was carried out at good ventilation conditions. The elemental compositions of the catalysts were measured using an energy dispersive X-ray (EDX) analyzer, which is attached to a JEOL MP5600LV

scanning electron microscope operating at 15 kV. Information on particle size, shape, and size distribution were obtained using a JEOL JEM2010 transmission electron microscope operating at 200 kV. X-ray photoelectron spectra were obtained using an ESCALAB MKII spectrometer (VG Scientific) with Al-K_α radiation (1486.71 eV). Spectral correction was based on the graphite C1s level at 284.5 eV. The vendor-supplied XPSPEAK version 4.1 was used to deconvolute the X-ray photoelectron spectroscopy (XPS) data by using fixed half widths and fixed spin-orbit splitting in first trials.

2.5. Electrochemical characterizations

An Autolab PGSTAT12 potentiostat/galvansotat and a standard three-electrode electrochemical cell were used to evaluate the catalysts via cyclic voltammetry. A catalyst ink was prepared by mixing 5 mg of the catalyst with 100 μL of Nafion (5 wt.% solution from Aldrich) and 900 μL of ethanol. The working electrode was a 5 mm diameter glassy carbon disk electrode cast with 10 μL of the catalyst ink (6.7 μg of the metal). Before ink casting, the electrode was routinely polished with 1.0, 0.3, and 0.05 mm Al_2O_3 paste and finally cleaned with ethanol solution in an ultrasonic bath. A Pt gauze and an Ag/AgCl (sat.) were used as the counter and reference electrodes, respectively. All potentials in this paper are quoted against an Ag/AgCl sat. electrode, which is 0.198 V versus a normal hydrogen electrode. The electrolytes used were 0.5 M H_2SO_4 and 1 M CH_3OH in 0.5 M H_2SO_4. A potential window of −0.18 V to 0.8 V (with respect to Ag/AgCl sat.) was scanned at 20 mV s^{-1} until a stable response was obtained before the voltammograms and chronoamperograms were recorded. The CO tolerance of the catalysts was evaluated via anodic stripping of the adsorbed CO. This process was done by saturating 0.5 M H_2SO_4 with 10% CO in Ar while the working electrode was held at −0.1 V for 30 min. The passage of CO was then stopped, and the electrolyte was thoroughly purged with high-purity Ar. CO stripping voltammograms were collected in the −0.18 V to 0.8 V potential window starting from −0.1 V.

3. Results and discussion

The polyol reduction method has been extensively applied for the preparation of tiny nanoparticles in the fuel cell community, in which ethylene glycol functions as a reducing agent and stabiliser. The viscosity of ethylene glycol is 25.66 mPa s (at 16 °C), which is higher than that of water (1.11 mPa s at16 °C). This property is conducive to the formation of small nanoparticles. In addition, the removal of ethylene glycol can be conducted by simply rinsing the product with water and ethanol. Thus, post-heat-treatment need not to be carried out. Fig. 1 shows the TEM image of the Os colloids prepared via the hydrothermal method. The particle sizes were very small (less than 1 nm) without obvious particle agglomeration, which indicates the successful reduction of the K_2OsO_6 precursor at the experimental condition. These Os colloids were further used for the reduction of Pt nanoparticle by refluxing in polyol solution, and the resulting TEM image of PtOs-2 colloids is shown in Fig. 2. Compared with those in Fig. 1, the particles in Fig. 2 significantly increased in size, and the average particle size was ~2 nm. However, determining whether the particles in Fig. 2 were mixtures of isolated Pt and Os nanoparticles or PtOs nanoparticles (alloys, bimetallic or core–shell structured nanoparticles) is difficult. Given the densities of Os and Pt, which are 22.4 and 21.4 g cm^{-3}, respectively, and assuming ideal spherical Os nanoparticles in Fig. 1 and Pt shell

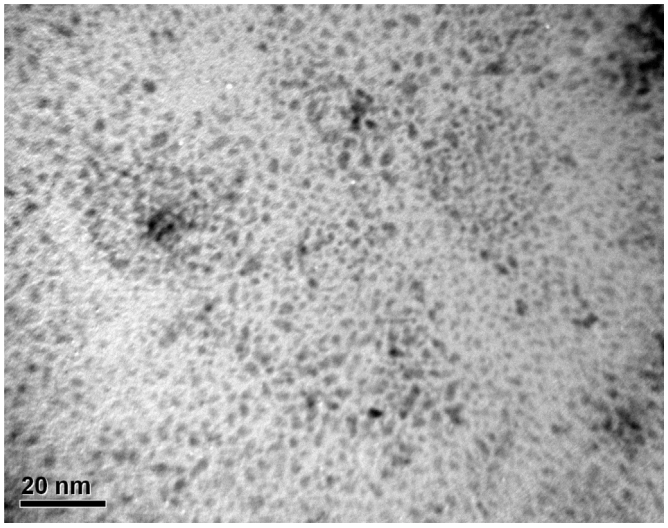

Fig. 2. TEM image of PtOs-2 colloids.

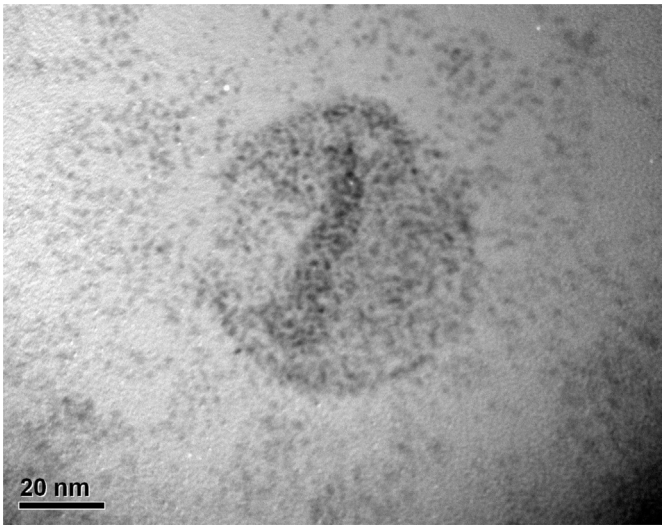

Fig. 1. TEM image of Os colloids.

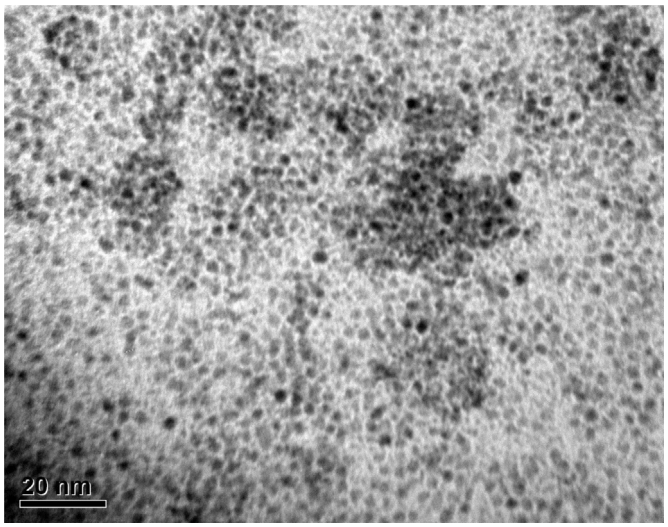

Fig. 3. TEM image of PtOs-1 colloids.

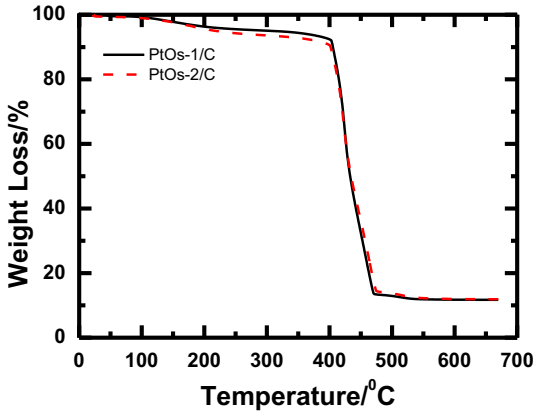

Fig. 4. Weight loss curves of the catalysts measured via TGA.

formation on Os core (Pt@Os) in Fig. 2, a purely theoretical calculation would require a Pt/Os mass ratio of 6.7:1. This finding is obviously not the case given that the nominal mass ratio is 3.1:1 (the atomic ratio of Pt/Os is preset at 3:1 and the mass ratio is calculated to be 3.1:1). Therefore, the particles observed in Fig. 2 must include isolated Os colloids with the rest being PtOs alloys or bimetallic nanoparticles. Fig. 3 presents the TEM image of PtOs-1, and the average particle size is larger than that in Fig. 2, which is around 2.5 nm. Considering the particles in Fig. 3 were formed via a co-reduction method, these particles are most likely PtOs alloyed nanoparticles.

Fig. 4 shows the weight loss curves of the catalysts measured via TGA. The weight loss of less than 10 wt.% in the samples between 100 °C and 400 °C could be attributed to the desorption of physisorbed water, whereas the weight loss between 400 °C and 473 °C was due to the combustion of carbon in air [27]. The remaining weight at 473 °C was 13.8 wt.% for both the catalysts, which is coincidently identical to that of the nominal loading of the catalysts (13.4 wt.%). The loadings calculated from the remaining weight after heating to 650 °C was 11.9 wt.% for both catalysts. The formation of OsO_4 leads to further weight decrease after $T > 473$ °C because OsO_4 is a gaseous species [22]. To confirm if Pt and Os precursors were completely reduced and harvested by the carbon support, EDX analysis of the catalysts were carried out. The results showed a Pt to Os ratio of 3:1 (a metal loading of ~14 wt.%) for both catalysts, which is in agreement with the starting molar ratio of the metals in the precursor salts. TGA was carried out at good ventilation conditions to avoid the release of toxic OsO_4 gas [25].

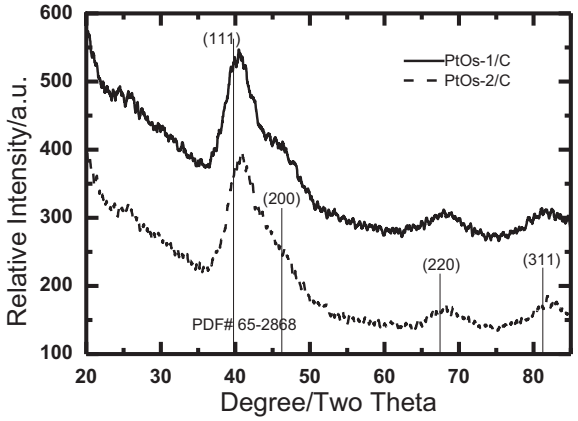

Fig. 5. XRD patterns of the catalysts.

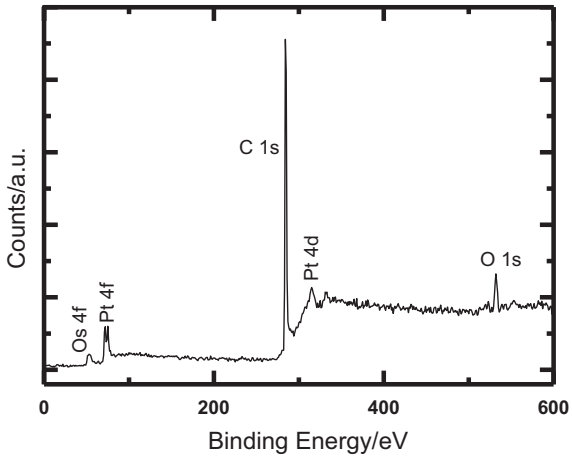

Fig. 6. A wide scan XPS spectrum from the PtOs-1/C electrocatalyst.

The XRD patterns of the catalysts are shown in Fig. 5. For both catalysts, the strong diffraction peaks at Bragg angles of 40.4°, 68.3°, and 81.9° can be indexed to the (111), (220), and (311) planes of face-centered cubic (f.c.c) platinum, respectively, which all shifted positively relative to those of pure Pt (PDF card# 65-2868) [28,29]. These findings are feasible for the PtOs-1/C catalyst because the co-deposition method led to the formation of the alloyed catalyst. For the PtOs-2/C catalyst, the two step sequential reduction process, which was employed for the synthesis of PtOs-2/C, might have also caused the partial formation of PtOs alloy or the PtOs structure. Combining the result with those obtained in TEM

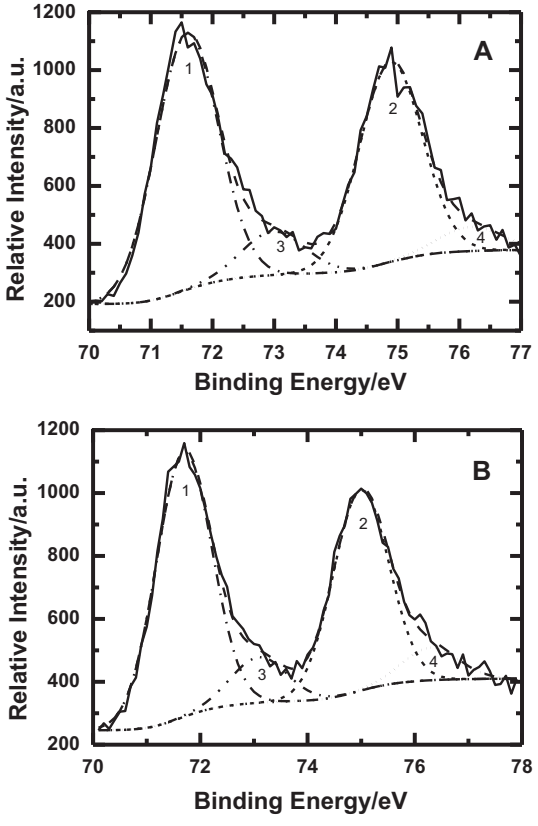

Fig. 7. Pt 4f X-ray photoelectron spectra from the electrocatalysts for (A) PtOs-1/C and (B) PtOs-2/C.

Table 1
Binding energies and relative integrated area intensities of component species deconvoluted from the Pt 4f XPS spectra.

Catalyst	Species	Binding energy (eV)	Relative integrated area intensity (%)	Sub-total (%)
PtOs-1/C	1 (Pt(0))	71.58	49	87
	2 (Pt(0))	74.88	38	
	3 (Pt(2))	72.98	8	13
	4 (Pt(2))	76.18	5	
PtOs-2/C	1 (Pt(0))	71.69	49	86
	2 (Pt(0))	74.99	37	
	3 (Pt(2))	73.09	8	14
	4 (Pt(2))	76.29	6	

Table 2
Binding energies and relative integrated area intensities of component species deconvoluted from the Os 4f XPS spectra.

Catalyst	Species	Binding energy (eV)	Relative integrated area intensity (%)	Sub-total (%)
PtOs-1/C	1 (Os(0))	51.24	36	67
	2 (Os(0))	53.94	31	
	3 (Os(2))	52.54	18	33
	4 (Os(2))	55.24	15	
PtOs-2/C	1 (Os(0))	51.08	49	87
	2 (Os(0))	53.78	38	
	3 (Os(2))	52.38	7	13
	4 (Os(2))	53.57	6	

analysis, PtOs-2 was deduced to contain a mixture of isolated Os and alloyed PtOs nanoparticles. The (200) diffraction peak was only observed in PtOs-1, whereas that for PtOs-2 was virtually not observable. This result is an indication of the relatively bigger particle size of PtOs-1 compared with that of PtOs-2. The volume-averaged particle size can be calculated from the Scherrer's equation [30,31] by using the Pt (220) peak for PtOs-1/C and PtOs-2/C, which are 2.1 and 2.7 nm, respectively. These values are in agreement with those obtained from the TEM observation.

The XPS spectrum of the PtOs-1/C catalyst consists of several major lines that can be indexed to Pt, Os, C, and O (Fig. 6). The Pt 4f spectra of PtOs-1/C and PtOs-2/C are shown in Fig. 7. In the deconvolution of the Pt 4f spectra, background removal was carried out via the Shirley baseline method, and both ends of the baseline were set far enough so that the spectra shape is not distorted. The XPS line shapes are a convolution of a Lorentzian, which is caused from both the natural exponential decay of the corehole states and the excitation radiation, and a Gaussian, which is caused by the analyzer system. In this work, the line shape was assumed to be Lorentzian, and the half widths were assumed to be equal. The only variables, therefore, were the relative intensities of the doublets as well as their splittings and positions. In the Pt 4f spectrum in Fig. 7(A) for PtOs-1/C, the more intense doublets at 71.58 and 74.88 eV are a characteristic of metallic Pt, and the less intense doublets at 72.98 and 76.18 eV are often assigned to oxidized Pt in divalent states such as PtO and Pt $(OH)_2$ [32]. The Pt 4f spectrum of PtOs-2/C (Fig. 7(B)) could be similarly deconvoluted, with the doublets at 71.69 and 74.99 eV assigned to Pt(0) and the doublets at 73.09 and 76.29 eV assigned to Pt(2). The percentages of Pt(0) in the catalysts calculated from the respective integrated area intensities are close to each other (87% for PtOs-1/C and 86% for PtOs-2/C). The binding energies of the Pt 4f components and the percentages of Pt(0) and Pt(2) in the catalysts calculated from the respective integrated area intensities are summarized in Table 1. From Table 1, the ratio of peak areas for the spin-orbit split double was 4:3 (Multiplet theory), which corresponds to the theoretical value [33,34]. The Os $4f_{7/2}$ and $4f_{5/2}$ binding energies for PtOs-1/C in Fig. 8(A) at 51.24 and 53.94 eV can be assigned to the Os metal and the binding energy peaks at 52.54 and 55.24 eV can be assigned to OsO_2 [33]. In the Os 4f spectrum for PtOs-2/C in Fig. 8(B), the metallic Os signals are at 51.08 and 53.78 eV, whereas the signals at 52.38 and 55.08 eV are assigned to the Os oxide (2). The binding energies of the Os 4f components and the percentages of Os(0) and Os(2) in the catalysts calculated from the respective integrated area intensities are shown in Table 2. A higher surface metallic Os content was observed for PtOs-2/C (87%) relative to that of PtOs-1/C (67%). This discrepancy

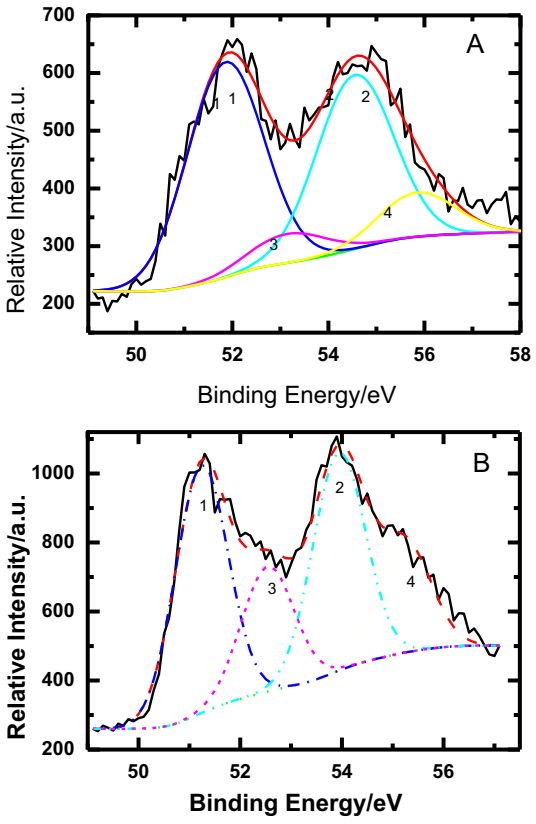

Fig. 8. Os 4f X-ray photoelectron spectra from the electrocatalysts for (A) PtOs-1/C and (B) PtOs-2/C.

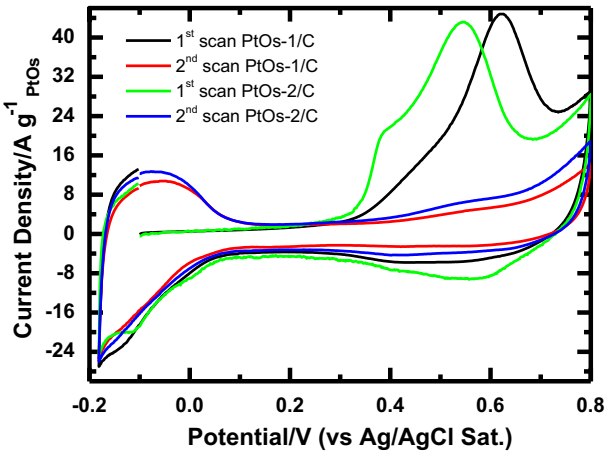

Fig. 9. CO stripping voltammograms in 0.5 M H_2SO_4 for the catalysts at room temperature (scan rate = 20 mV s^{-1}).

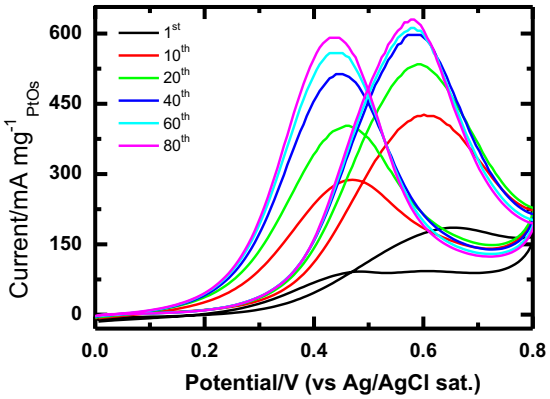

Fig. 10. Cyclic voltammograms of methanol electrooxidation for the PtOs-2/C catalyst in 1 M CH_3OH + 0.5 M H_2SO_4 measured at 20 mV s^{-1} at room temperature.

might be caused by the different fabrication methods because PtOs-2/C was prepared via a sequential reduction method, in which preformed Os colloids were less prone to oxidization. The atomic ratios from the XPS analysis of PtOs-1/C and PtOs-2/C were 3.1:1 and 2.8:1, respectively. These findings are acceptable given that the ratio from the XPS result is virtually the same as that from the EDX result because of its small size effect. The increase in Pt binding energy (71.58 eV for PtOs-1/C versus 71.69 eV for PtOs-2/C) and the corresponding decrease in Os binding energy (51.24 eV for PtOs-1/C versus 51.08 eV for PtOs-1/C) for PtOs-2/C indicate an electron transfer effect from Os to Pt, which appears to correlate with the lower OsO_2 in PtOs-2/C.

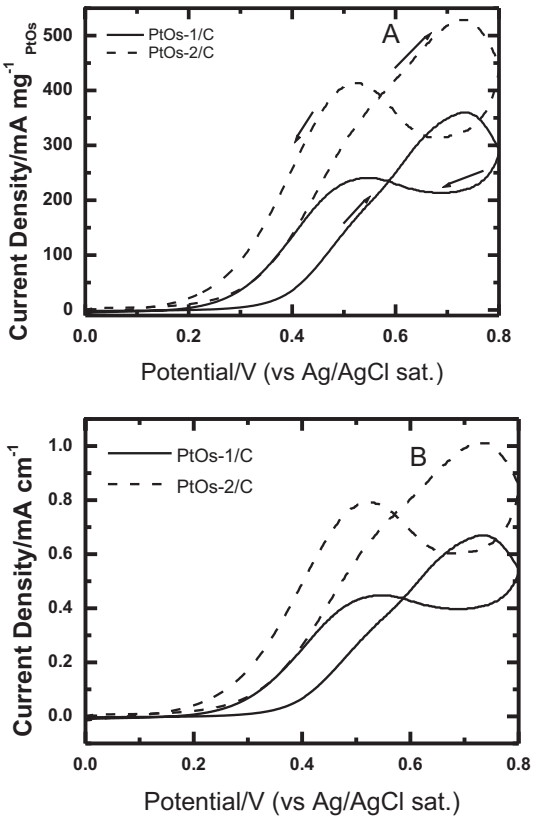

Fig. 11. Cyclic voltammograms of methanol electrooxidation for the catalysts in 1 M CH_3OH + 0.5 M H_2SO_4 measured at 20 mV s^{-1} at room temperature.

Table 3
Comparison of the methanol oxidation activities for the catalysts.

Catalyst	Forward current density at peak potential (I_f)/mA mg^{-1}_{PtOs}	Backward current density at peak potential (I_b)/mA mg^{-1}_{PtOs}	Ratio (I_f/I_b)
PtOs-1/C	528	352	1.5
PtOs-2/C	361	278	1.3

The upper potential limit was set at 0.8 V to avoid possible Os dissolution and oxidation from the catalysts [24,33]. Fig. 9 presents the CO stripping voltammograms in 0.5 M H_2SO_4 for the catalysts at room temperature. CO stripping is commonly known to be an effective electrochemical tool for the characterization of CO tolerance [35,36]. The general voltammetric features are in agreement with those in literature, in which CO oxidation was completed in the first scan without any trace of CO in the second scan [14,37]. The CO onset and peak oxidation potentials for PtOs-1/C are 0.32 and 0.63 V, respectively, whereas those for PtOs-2/C are 0.28 and 0.55 V, respectively, both of which negatively shifted relative to those of PtOs-1/C. The considerably negative CO onset potentials were certainly caused by the well-known bifunctional effect. In addition, a pre-oxidation peak was observed at 0.38 V for PtOs-2/C. The negative shift of CO onset potential and peak stripping potential for PtOs-2/C implies the greater ease of CO removal and improved CO tolerance. The multiple CO oxidation peaks for PtOs-2/C were attributed to the mixed components (possibly isolated Os, PtOs alloy, or bimetallic nanoparticles), as discussed in TEM and XRD analysis section. The easier CO stripping performance of PtOs-2/C was probably due to the higher metallic Os content, which is similar to the XPS analysis results (87% for PtOs-2/C versus 67% for PtOs-1/C). Therefore, the physical characteristics of PtOs-2/C and its CO stripping electrochemical behaviors correlated well with each other. The electrochemically active surface area (ECSA) of the electrocatalysts is often estimated from the charge associated with hydrogen adsorption or desorption on Pt in an acidic electrolyte. Based on the second scan in Fig. 9, the ECSAs of PtOs-1/C and PtOs-2/C were close to each other at 52 and 54 $m^2\ g^{-1}$, respectively. Our hypothesis is that ethylene glycol or its oxidizing species might still remain on the catalyst surface even after copious rinsing.

Fig. 10 displays the cyclic voltammetric profile with increasing scan number in 0.5 M H_2SO_4 + 1 M CH_3OH at 20 mV s^{-1} for PtOs-2/C. With the increase of scan number, the oxidation current increases and stabilizes after 40 cycles. The catalytic activities toward

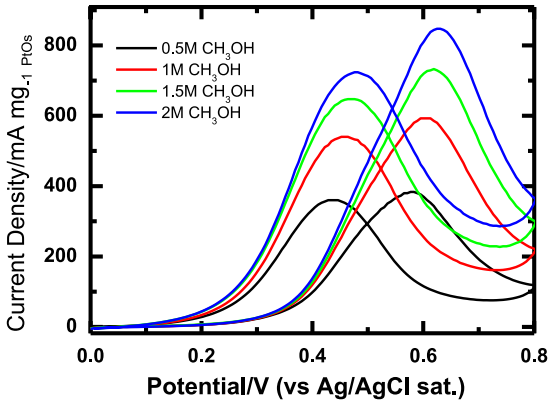

Fig. 12. Cyclic voltammograms of methanol electrooxidation for the PtOs-2/C catalyst measured at different methanol concentrations in 0.5 M H_2SO_4 at 20 mV s^{-1} at room temperature.

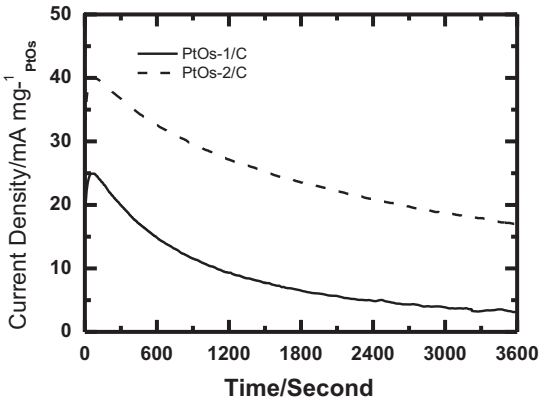

Fig. 13. Chronoamperograms of the electrocatalysts biased at 0.4 V in 1 M CH_3OH + 0.5 M H_2SO_4 at room temperature.

methanol oxidation reaction at room temperature were evaluated via cyclic voltammetry in 0.5 M H_2SO_4 + 1 M CH_3OH at 20 mV s^{-1}, as shown in Fig. 11. To fairly evaluate the electrocatalysts, the current densities in Fig. 11(A) were normalized to the metal loading, which indicate the mass activity of the electrocatalysts, whereas the current densities in Fig. 11(B) were normalized to the ECSA, which indicate the intrinsic activity of the catalysts' active sites (specific activity) [38]. The PtOs-2/C electrocatalyst had a mass activity (Fig. 11(A)) and specific activity (Fig. 11(B)) of 528 mA mg^{-1}_{PtOs} and 0.98 mA cm^{-2}, respectively, which are 46% and 42% higher than those of the PtOs-1/C electrocatalyst (361 mA mg^{-1}_{PtOs} in Fig. 11(A) and 0.69 mA cm^{-2} in Fig. 11(B)). The ratios of the forward peak current density to the backward one for PtOs-1 and PtOs-1 are all greater than 1 (Table 3) and these are indications of good CO tolerance for the home-made catalysts. To investigate the effect of concentration on the catalytic activity, the catalytic activity of PtOs-2/C was tested when CH_3OH concentration changed from 0.5 M to 2 M and this was shown in Fig. 12. It was found that the oxidation current increases with the increase of concentration and the peak potential also shifted to positive potentials. The mass activity of PtOs-2/C reached 850 mA mg^{-1}_{PtOs} in 0.5 M H_2SO_4 + 2 M CH_3OH.

Fig. 13 compares the chronoamperograms (CA) of the catalysts at 0.4 V. When the potential was biased at 0.4 V, methanol was continuously oxidized on the catalyst surface, and reaction intermediates would accumulate if the kinetics of their removal reaction could not match the kinetics of methanol oxidation. A more gradual decay of current density with time is nevertheless an indication of improved CO resistance. The oxidation current density decreased to 43% of its initial value after 1 h for the PtOs-2/C catalyst, whereas the corresponding decay for the PtOs-1/C catalyst was more severe at 13%. This CA result was also in good agreement with that obtained in the CO stripping.

4. Conclusions

PtOs-1/C electrocatalyst was prepared via a co-reduction method and was compared with PtOs-2/C, which was synthesized by the deposition of Pt over preformed Os colloids. The results show a strong effect of the preparation method on the composition, particle size, and oxidation states of the electrocatalysts, as well as the electrochemical performance for methanol oxidation reaction. The mass and specific activities of PtOs-2/C are 528 mA mg^{-1}_{PtOs} and 0.98 mA cm^{-2}, respectively, which are 46% and 42% higher than those of PtOs-1/C. The former catalyst also had a higher CO tolerance and stability than the latter.

Acknowledgments

Jianhuang Zeng acknowledges the Project on the National Natural Science Foundation-Guangdong Joint Foundation (U1301245), the Project on the Integration of Industry, Education and Research of Guangdong Province (2012B091100144), the Fundamental Research Funds for the Central Universities (2013ZZ0064), and Zuopeng Li thanks Shanxi Province Science Foundation for Youths (2012021006-1) for the financial supports of this work.

References

[1] S.M.M. Ehteshami, S.H. Chan, Electrochim. Acta 93 (2013) 334–345.
[2] X. Zhao, M. Yin, L. Ma, L. Liang, C.P. Liu, J. Liao, T.H. Lu, W. Xing, Energy Environ. Sci. 4 (2011) 2736–2753.
[3] Serov, C. Kwak, Appl. Catal. B Environ. 90 (2009) 313–320.
[4] N.V. Rees, R.G. Compton, J. Solid State Electrochem. 15 (2011) 2095–2100.
[5] K. Sasakia, J.X. Wang, H. Naohara, N. Marinkovic, K. More, H. Inada, R.R. Adzic, Electrochim. Acta 55 (2010) 2645–2652.
[6] M. Shao, K. Sasakia, N.S. Marinkovicb, L. Zhang, R.R. Adzic, Electrochem. Commun. 9 (2007) 2848–2853.
[7] D.-H. Lim, W.-D. Lee, D.-H. Choi, H.-In Lee, Appl. Catal. B Environ. 94 (2010) 85–96.
[8] A. Chen, P. Holt-Hindle, Chem. Rev. 110 (2010) 3767–3804.
[9] R. Dillona, S. Srinivasana, A.S. Aricòb, V. Antonuccib, J. Power Sources 127 (2004) 112–126.
[10] A.S. Arico, S. Srinivasan, V. Antonucci, Fuel Cells 1 (2001) 1–29.
[11] S. Wasmus, A. Kuver, J. Electroanal. Chem. 461 (1999) 14–31.
[12] Y.X. Li, L.P. Zheng, S.J. Liao, J.H. Zeng, J. Power Sources 196 (2011) 10570–10575.
[13] F. Ye, J.H. Yang, W.W. Hu, S.J. Liao, J.H. Zeng, J. Yang, RSC Adv. 2 (2012) 7479–7486.
[14] Y.-C. Hsieh, L.-C. Chang, P.-W. Wu, Y.-M. Chang, J.-F. Lee, Appl. Catal. B Environ. 103 (2011) 116–127.
[15] J.H. Zeng, M.J. Han, X.Y. Lu, D. Chen, S.J. Liao, Electrochim. Acta 112 (2013) 431–438.
[16] J.H. Zeng, J.Y. Lee, J. Power Sources 140 (2005) 268–273.
[17] J.H. Zeng, J.Y. Lee, Int. J. Hydrogen Energy 32 (2007) 4389–4396.
[18] B. Gurau, R. Viswanathan, R.X. Liu, T.J. Lafrenz, K.L. Ley, E.S. Smotkin, E. Reddington, A. Sapienza, B.C. Chan, T.E. Mallouk, S. Sarangapani, J. Phys. Chem. B 102 (1998) 9997–10003.
[19] M.H. Atwan, D.O. Northwood, E.L. Gyenge, Int. J. Hydrogen Energy 30 (2005) 1323–1331.
[20] W. Liu, J. Huang, J. Power Sources 189 (2009) 1012–1015.
[21] E.I. Santiago, E.A. Ticianelli, Int. J. Hydrogen Energy 30 (2005) 159–165.
[22] M.B. de Oliveira, L.P.R. Profeti, P. Olivi, Electrochem. Commun. 7 (2005) 703–709.
[23] J. Huang, H. Yang, Q. Huang, Y. Tang, T. Lu, D.L. Akins, J. Electrochem. Soc. 151 (2004) A1810–A1815.
[24] Y. Zhu, C.R. Cabrea, Electrochem. Solid-state Lett. 4 (2001) A45–A48.
[25] J.T. Moore, D. Chu, R. Jiang, G.A. Deluga, C.M. Lukehart, Chem. Mater. 15 (2003) 1119–1124.
[26] Z. Zhou, S. Wang, W. Zhou, G. Wang, L. Jiang, W. Li, S. Song, J. Liu, G. Sun, Q. Xin, Chem. Commun. 3 (2003) 394–395.
[27] F.B. Su, J.H. Zeng, Y. Yu, L. Lv, J.Y. Lee, X.S. Zhao, Carbon 43 (2005) 2366–2373.
[28] J.H. Zeng, J. Mate. Chem. 22 (2012) 3170–3176.
[29] Y.Y. Chua, Z.B. Wang, Z.Z. Jiang, D.M. Gu, G.P. Yin, J. Power Sources 203 (2012) 17–25.
[30] S. Zhang, Y. Shao, G.P. Yin, Y.H. Lin, J. Mater. Chem. 20 (2010) 2826–2830.
[31] S. Zhang, Y. Shao, G.P. Yin, Y.H. Lin, Appl. Catal. B Environ. 102 (2011) 372–377.
[32] J. Xu, G. Fu, Y. Tang, Y. Zhou, Y. Chen, T.H. Lu, J. Mater. Chem. 22 (2012) 13585.
[33] R. Liu, H. Iddir, Q. Fan, G. Hou, A. Bo, K.L. Ley, E.S. Smotkin, Y.-E. Sung, H. Kim, S. Thomas, A. Wieckowski, J. Phys. Chem. B 104 (2000) 3518–3531.
[34] J.B. Goodenough, A. Hamnett, B.J. Kennedy, S.A. Weeks, Electrochim. Acta 32 (1987) 1233–1238.
[35] P. Ochala, J.L.G. de la Fuentea, M. Tsypkina, F. Selanda, S. Sundea, N. Muthuswamy, M. Rønning, D. Chen, S. Garcia, S. Alayoglu, B. Eichhorn, J. Electroanal. Chem. 655 (2011) 140–146.
[36] T.Y. Jeon, S.J. Yoo, Y.H. Cho, H.Y. Park, Y.E. Sung, Electrochem. Commun. 28 (2013) 114–117.
[37] L. Feng, F. Si, S. Yao, W. Cai, W. Xing, C. Liu, Catal. Commun. 12 (2011) 772–775.
[38] J.H. Zeng, J.Y. Lee, J. Chen, P.K. Shen, S. Song, Fuel Cells 7 (2007) 285–290.